Trends and Development of Sliding Mode Control Applications for Renewable Energy Systems

Yun Yang and Siew Chong Tan *

Department of Electrical and Electronic Engineering, The University of Hong Kong, Hong Kong, China
* Correspondence: sctan@eee.hku.hk; Tel.: +852-3917-2707

check for
updates

Abstract: Based on the matured theoretical framework of sliding mode control for varied, nonlinear, and unpredictable systems, practical designs of sliding mode control have been developed to suit the purpose of controlling power converters under various operating conditions. These design guidelines are particularly valuable for emerging technologies with renewable energy sources. This paper presents a discussion on the recent development of sliding mode control applications for renewable energy systems, and further examines the current trends of achieving efficiency improvement of renewable energy systems and load protections against large overshoot/undershoot in transient states, by utilizing the fast-dynamic-tracking capability of the sliding mode control. Three comparative case studies between the sliding mode control and proportional-integral control involving, namely, a low-power wind energy conversion system, a series-series-compensated wireless power transfer system, and a multiple energy storage system in a direct current (DC) microgrid, are provided.

1. Introduction

The sliding mode (SM) control is a unique type of nonlinear control that is particularly suited for variable structure systems. Its control mechanism involves a state-feedback discontinuous control law that continuously actuates the controlled system to abruptly change its operation from one continuous state to another, at high frequency, such that the controlled system's dynamics are constricted to following a particular reference track. In so doing, superior large-signal control responses and small-signal stability of systems with significant parameter uncertainties and large operating point changes are more easily achievable with SM control compared to other control approaches [1]. Additionally, the advantages of SM control compared to other nonlinear control methods include being generally free of online system identification and ease of implementation.

Since the early development of variable structure control in the 1950s and 1960s [2–4], various branches of SM control, including discrete SM control, adaptive SM control, terminal SM control, and global SM control, etc., have been investigated for nonlinear systems, infinite-dimensional systems, multiple-input-multiple-output systems, stochastic systems, discrete systems, and variable structure systems, etc. [5–12]. V. I. Utkin surveyed a class of variable structure systems in 1977 [5]. S. Z. Sarpturk et al. demonstrated the control input must be upper and lower bounded for discrete SM control [6]. H. Sira-Ramirez et al. combined the advantages of chattering-free dynamic SM control and the adaptive backstepping technique to regulate linearizable systems [7]. G. Wheeler et al. improved the adaption law on the upper bound of uncertainties to guarantee the boundness of both states of the plant and the estimated control gains [8]. Y. Feng et al. presented a new terminal sliding mode manifold for the second-order system to resolve the singularity issue associated with

the conventional terminal SM control [9]. H. S. Choi et al. proposed a global SM control with the consideration of input disturbances and uncertainties of the parameters to ensure sliding behavior throughout an entire response for motor drives. In that study, the SM control further enhanced the dynamic tracking performance by minimizing the reaching time of the sliding surface [10]. The neural network learning is achieved with an online adaption algorithm that inherits robustness and high-speed learning from the SM control. Y. S. Lu et al. proposed a self-organizing fuzzy SM control to achieve rapid and accurate tracking of a class of nonlinear systems [11]. B. Yoo et al. adopted fuzzy logic approximators to approximate the unknown system functions in designing the SM control of nonlinear systems [12]. Since then, most SM control works have been redirected toward exploring potential real-life utilizations, of which their applications in switching power converters is one area that has been most extensively studied.

The earliest publication on SM control of power converters can be traced back to 1983 by F. Bilalović, where the feasibility of using SM control for buck converters was examined [13]. This was followed by R. Venkataramanan et al., who presented comprehensive applications of equivalent SM control on basic second-order DC-DC converters to achieve constant-frequency SM control [14]. Since then, SM control for higher-order and more complex topologies and configuration of converters have been exhaustively studied [15–24], including that of L. Martínez-Salamero et al. and P. Mattavelli et al., who proposed design methods for achieving locally-stable SM control for high-order converters [18,19]. In addition, the works covering the performance evaluation of SM controlled DC-DC converters include that of G. Escobar et al. [25] and S. C. Tan et al. [1], who compared and validated the superior dynamic tracking performance of the SM control over other controls. Further, S. P. Huang et al. applied the SM control on a fourth-order Ćuk converter in 1989 [15]. E. Fossas et al. investigated the audio-susceptibility and load disturbance of a Ćuk converter controlled by SM control [16]. L. Malesani et al. summarized the SM control designs for the Ćuk converter [17]. M. Castilla et al. presented an SM control for quantum resonant converters [20]. P.F. Donoso-Garcia et al. and Y.B. Shtessel et al. proposed the use of SM control to regulate the output voltage and balance the current of modular DC-DC converters [21]. M. López et al. and R. Giral et al. applied the SM control for interleaving parallel-connected boost-type modular converters [22]. M. López et al. also designed an SM control, which is more relevant to practical power converters, for parallel-connected boost converters [23].

The pioneering works on SM control of power converters have laid a strong foundation for the subsequent works on SM control of renewable energy systems. Most renewable energy systems are linked to or contain power electronics components as part of their systems. By far, SM control has been diversely applied to the power electronics components in renewable energy systems to improve the power system's quality and dynamic responses. This is particularly appropriate since many renewable sources are intermittent, largely fluctuating, and highly uncertain in nature. Further, achieving good power quality, such as high voltage and frequency stability, high power factor, and low voltage and current harmonics, has always been the primary pursuit in such applications.

For the reasons above, most earlier investigations on SM control of renewable energy systems were focused solely on their power quality enhancement [26–32]. In [26], the stabilization of the voltage amplitude and frequency was attained via the mitigation of the power imbalance between the power supply and demand in the presence of appreciable wind power generation using SM control. In [27], the SM control was adopted in dedicated local controllers of wind energy conversion (WEC) systems, smart loads, and energy storage systems (ESS) to robustly regulate the power flow and direct current (DC) bus voltage, even in the presence of model uncertainties and external disturbances. In [28], the SM control was designed for both positive and negative sequence power control to improve the power sharing and harmonics cancellation of a hybrid AC/DC microgrid. In [29], a double SM frequency control strategy with a disturbance observer was applied to an isolated hybrid micro-grid to achieve frequency regulation. The control method can significantly reduce frequency deviation and maintain the power balance of the plant even with unmatched uncertainties and resource variations. In [30], the fixed-frequency SM control was applied to a voltage-fed quasi-Z-source inverter to ensure

stable operation of the battery storage system with a variable renewable energy source. In [31], a second-order SM controller was implemented to regulate the zero-sequence injection of a four-leg three-level neutral-point-clamped inverter to control the power flow of a hybrid ESS, which comprises a lithium-ion battery and a vanadium redox flow battery. The controller manages the hybrid ESS in terms of improving the power quality and stability, and also performs the control of the renewable energy injection into a microgrid. In [32], a high-order SM controller was adopted to ensure the stability of a wind turbine in the presence of parametric uncertainties of the turbine, as well as electric grid disturbances.

In more recent works, the state-of-the-art research on SM control of renewable energy systems involve, in addition to achieving high power quality, the dynamic tracking improvement of the renewable energy systems. By far, several investigations have been carried out to showcase the advantages of SM control over linear control in dynamic power tracking of the systems with renewables [33–39]. In [35], a reduced-order SM controller was designed for a cascaded boost converter in a photovoltaic (PV) system to achieve a high conversion ratio with an efficiency of close to 95% for a wide operating range. The reduced-order SM control is derived based on the full-order switched model of the cascaded boost converter, taking into account the sliding mode constraints, the nonlinear characteristic of the PV module, and the dynamics of the maximum power point tracking (MPPT) controller. In [36], the boundary control with variable sliding surfaces was adopted in the MPPT controller to attain maximum power extraction from PV cells in dynamic conditions. It is found that significant improvement is achievable over conventional proportional-integral (PI) control. In [37], SM control was applied to both the mechanical system and the power converter of a low-power WEC system in a DC microgrid. Compared to the conventional MPPT schemes using linear controllers, the SM control regulates the dynamics of the WEC system more rapidly and achieves better energy harvesting. This is due to the fast-dynamic-tracking merit of SM control, which significantly improves dynamic energy-harvesting property as compared to linear controllers in conditions of variable sun and wind. In [38], a pulse-width-modulation (PWM)-based SM control was applied to the buck-boost regulator of the series-series (SS)-compensated wireless power transfer (WPT) system with variable power generations and consumptions. The PWM-based SM control exhibits better dynamic tracking performance of the output voltage than the conventional linear control when the input voltage, the mutual inductance, or the load condition of the WPT system is variable. In [39], an SM control-based direct power control (DPC) was designed for a dual-active-bridge (DAB) DC-DC converter, which has been widely adopted in DC and hybrid microgrids, to achieve accurate reference tracking against line and load disturbances, as well as low overshoot and undershoot in dynamics.

Clearly, the intentional exploitation of the advantage of fast dynamic tracking of SM control can further result in more energy harvesting of renewable energy sources and possibly better load protections for various renewable energy systems. This could be a trend for future SM control applications in renewable energy systems. In this paper, through the illustrations of some case studies, an examination is provided of how the emerging use of SM control is extendable to such complex renewable power-electronics systems and how their advantages can be significant in such applications.

2. Case Study 1-SM Control for Low-Power WEC Systems in DC Microgrids

In [37], the absolute MPPT of a low-power WEC system without energy storage was achieved only if the power consumption of the load fully matched the maximum power generation of the wind turbine. In practice, wind energy is intermittent. To achieve real-time MPPT of the WEC system, both the power generation and the consumption are required to be dynamically and instantaneously matched. The quicker the power generation matches the consumption, the higher the amount of energy that can be extracted for the time period. This section presents the application of SM control on both the wind turbine and its subsequent grid-connected converter in achieving fast dynamic power tracking of a low-power WEC system in a DC microgrid in maximizing its harvested energy.

The schematic diagram of the system in the case study is shown in Figure 1. The WEC system consists of a wind turbine system and a power conversion system. The wind turbine system extracts the maximum power from the wind and converters it into electrical power, which is further converted by the power conversion system to feed the DC grid with proper control. Specifically, the torque of the wind turbine is controlled by the MPPT controller-1 via the regulation of the output voltage (i.e., E_{rmf}) of the generator, thus the maximum power generation (MPG) from wind energy can be implemented. However, by only adopting the MPPT controller-1, the wind turbine system cannot guarantee all the generated power being injected into the DC grid without using any local ESS. The MPPT controller-2 needs to be used for the power conversion system to achieve maximum power injection (MPI) based on the state feedback signals of $V_{DC\text{-link}}$, i_{R2}, and v_C, such that the injected power into the DC grid matches the MPG.
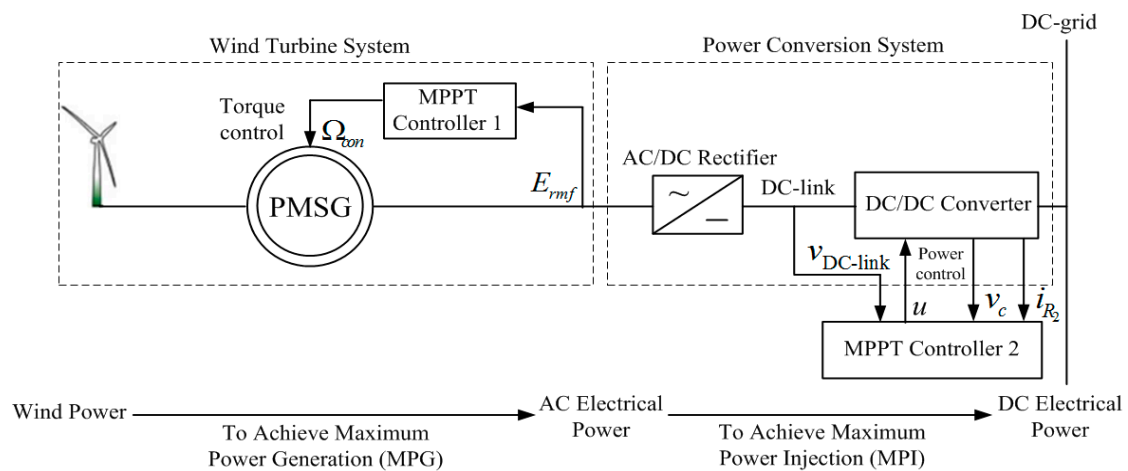
Figure 1. Schematic diagram of a low-power wind energy conversion (WEC) system in a DC microgrid.

For the wind turbine system, the mechanical equation of the shaft is:

$$J\frac{d\Omega}{dt} = T_g - T_e - f\Omega \tag{1}$$

where J is the total moment of inertia; Ω is the mechanical generator speed; T_g is the gearbox torque; T_e is the electrical torque; and f is the viscous friction coefficient. The mechanical generator speed reference is:

$$\Omega_{ref} = \frac{\lambda_{opt}vG}{R} \tag{2}$$

where R is the radius of the blade; G is the gear ratio of the gear box; v is the speed of wind; and λ_{opt} is the optimal tip ratio for the maximum conversion ratio. Obviously, the MPG of the wind turbine system can be implemented by tracking the mechanical generator speed reference. Then, the sliding surface of the SM control for the MPPT controller-1 can be selected as:

$$S = \dot{\Omega}_{ref} - \dot{\Omega} + c(\Omega_{ref} - \Omega) \tag{3}$$

where c is a tuning coefficient. By substituting (1) and (2) into (3),

$$S = \left(\frac{f^2}{J^2} + \frac{cf}{J}\right)S + \left(\frac{f}{J^2} + \frac{c}{J}\right)(T_e - T_g) + \ddot{\Omega}_{ref} + c\dot{\Omega}_{ref} - \left(\frac{f^2}{J^2} + \frac{cf}{J}\right)\Omega_{ref} \tag{4}$$

To satisfy the criteria $S \cdot \dot{S} < 0$, the control signal of the SM control for the MPPT controller-1 can thus be derived as:

$$\Omega_{\text{con}} = f\Omega_{\text{ref}} - \alpha_1 \ddot{\Omega}_{\text{ref}} - \left(J - \frac{f}{J}\alpha_1\right)\dot{\Omega}_{\text{ref}} - \alpha_2 \text{sgn}(\Omega_{\text{ref}} - \Omega) \tag{5}$$

where sgn (.) indicates the signum function; and α_1 and α_2 are the sliding coefficients.

Alternatively, the control signal of the conventional PI control for the MPPT controller-1 is:

$$\Omega_{\text{con}} = K_{\text{p}}(\Omega_{\text{ref}} - \Omega) + K_{\text{i}} \int_o^t (\Omega_{\text{ref}} - \Omega)dt \tag{6}$$

where K_{p} and K_{i} are the proportional and integral gains. In this paper, the sliding coefficient α_2 of the adopted

SM control and the tuning coefficients K_{p} and K_{i} of the PI control are tuned by the trial-and-error method. The sliding coefficient α_1 of the SM control satisfies:

$$\alpha_1 = \frac{J^2}{cJ + f} \tag{7}$$

For the power conversion system, the state-space equation of the grid-connected converter is:

$$\begin{cases} v_{\text{DC-link}}u = L_1\frac{di_{L_1}}{dt} + R_1 i_{L_1} + v_c \\ v_{\text{DC-grid}} = -R_2 i_{L_1} + R_2 C\frac{dv_c}{dt} + v_c \end{cases} \tag{8}$$

The sliding surface of the SM control for the MPPT controller-2 is chosen as:

$$S(x,t) = \sum_{i=1}^{3} \alpha_i x_i(t) \tag{9}$$

where α_i indicates the sliding coefficients and $x_i(t) \in x(t)$. Besides,

$$x = \begin{bmatrix} x_1 \\ x_2 \\ x_3 \end{bmatrix} = \begin{bmatrix} V_{\text{ref}} - \beta v_c \\ \frac{d(V_{\text{ref}} - \beta v_c)}{dt} \\ \int (V_{\text{ref}} - \beta v_c)dt \end{bmatrix} \tag{10}$$

Then, by substituting (8) into (10), the control signal of the SM control for the MPPT controller-2 can be derived as:

$$v_{\text{con}} = K_1 i_c + K_2 v_c + K_3 \tag{11}$$

and

$$|v_{\text{ramp}}| = \beta v_{\text{DC-link}} \tag{12}$$

where $K_1 = -\frac{\alpha_1 \beta L_1}{\alpha_2} + \beta\left(\frac{L_1}{R_2 C} + R_1\right)$, $K_2 = -\frac{\alpha_3 \beta L_1 C}{\alpha_2} + \beta\left(\frac{R_1}{R_2} + 1\right)$, and $K_3 = -\frac{\beta R_1}{R_2}V_{\text{DC-grid}} + \frac{\alpha_3}{\alpha_2}L_1 C\left(\frac{P_{\text{ref}}v_{\text{DC-link}}}{V_{\text{DC-grid}}}R_2 + V_{\text{DC-grid}}\right)$, which are tuned to satisfy the hitting, existence, and stability conditions of sliding mode operation. The sliding coefficients satisfy $\alpha_1 > 0$, $\alpha_2 > 0$, and $\alpha_3 > 0$ to ensure the Hurwitz-Routh stability of the sliding surface. Alternatively, the control signal of the conventional PI control for the MPPT controller-2 is:

$$v_{\text{con}} = K_{\text{p}}(v_{\text{ref}} - \beta v_c) + K_{\text{i}} \int_o^t (v_{\text{ref}} - \beta v_c)dt \tag{13}$$

and

$$|v_{\text{ramp}}| = \text{constant} \tag{14}$$

Then, the duty cycle of the grid-connected converter for both control is:

$$d = \frac{v_{\text{con}}}{|v_{\text{ramp}}|} \tag{15}$$

The sliding coefficients α_1, α_2, and α_3 of the SM control are tuned based on the guidelines in [1]. The tuning coefficients K_p and K_i of the PI control are tuned by the trial-and-error method.

The comparisons are conducted in experiments between the SM controllers and the conventional PI controllers for the wind turbine system with MPG, the power conversion system with MPI, and the entire WEC system with MPPT. With practical considerations, the wind speed is constrained within 6.6 m/s to 7.9 m/s. For the wind turbine system with MPG, the waveforms of the output voltage, the output current, and the output power of the wind turbine controlled by the conventional PI control and SM control are presented in Figure 2a,b, respectively. Here, both the PI control and SM control are optimally tuned under this wind speed change condition. The output power over the two transient cycles is approximately 430.7 W for the PI control and 431.6 W for the SM control. The difference of the extracted power between the two controls is quite small.

(**a**) Conventional PI control　　　　　　　　　　　(**b**) SM control
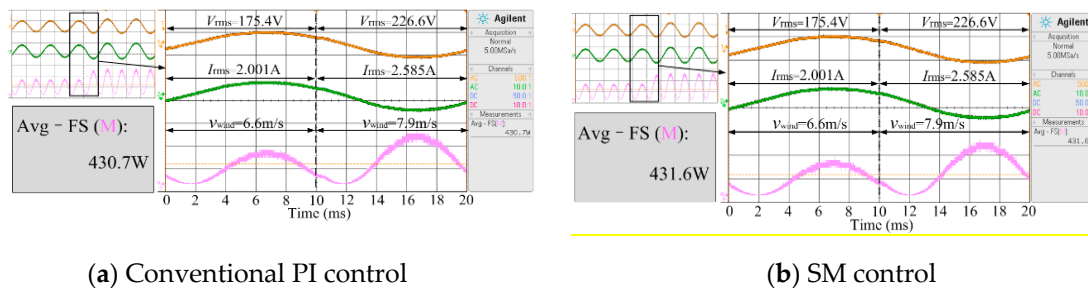
Figure 2. The experimental waveforms of the output voltage, the output current, and the output power of wind turbine system for wind speed altering from 6.6 to 7.9 m/s.

For the power conversion system with MPI, the root-mean-square (RMS) value of the input AC voltage is altered from 180 V to 220 V to simulate a step change in wind energy. The experimental waveforms of the DC grid voltage and the output power of the grid-connected converter controlled by the conventional PI control and SM control, are shown in Figure 3a,b. Here, both the PI control and SM control are optimally tuned under this voltage change condition. The settling time of the output power for both control are identical at 15.8 ms.

(**a**) Conventional PI control　　　　　　　　　　　(**b**) SM control
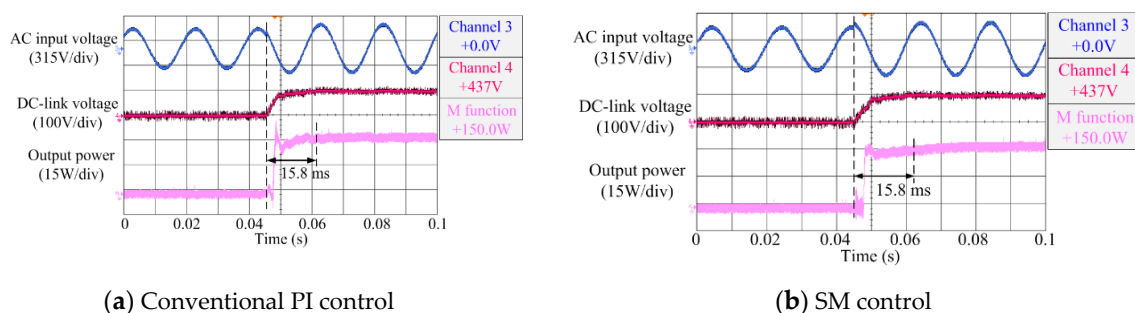
Figure 3. The experimental waveforms of the DC grid voltage and the output power of the power conversion system for input voltage changing from 180 to 220 V.

Then, with both the PI control and SM control settings kept in the abovementioned tuned values, the MPPT performance of the entire system is evaluated. Various experiments are performed with the wind speed first changing from 7.9 m/s to 6.6 m/s and then from 6.6 m/s back to 7.9 m/s. The corresponding waveforms are shown in Figure 4. From Figure 4a,b, it can be seen that the SM control takes a shorter time of 11.1 ms to reach the steady state MPPT position as compared to the PI

control, which takes approximately 16.8 ms (about 34% more time), when there is a step change of wind speed from 6.6 m/s to 7.9 m/s. For the case of stepping down the wind speed from 7.9 m/s to 6.6 m/s, the SM control is also quicker in responding to the change with settling time of 30.1 ms, as compared to that of PI control at 43.7 ms (about 45% more time). The experiments were also conducted for the case of the wind speed changing from 7.3 m/s to 6.6 m/s and then from 6.6 m/s back to 7.3 m/s (results not included in paper). All results validate that the WEC system with SM control tracks faster the MPPT position, and thus presumably harvests more energy than conventional linear controllers on account of faster dynamics.

(**a**) Conventional PI control   (**b**) SM control

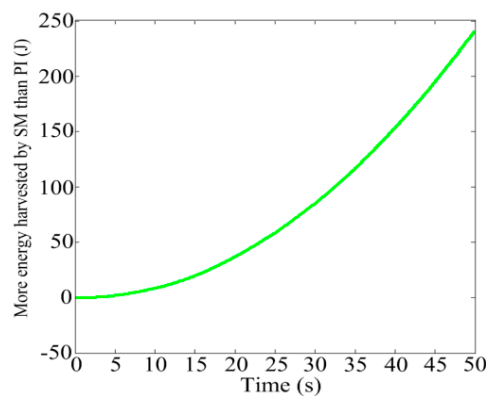(**c**) Conventional PI control   (**d**) SM control
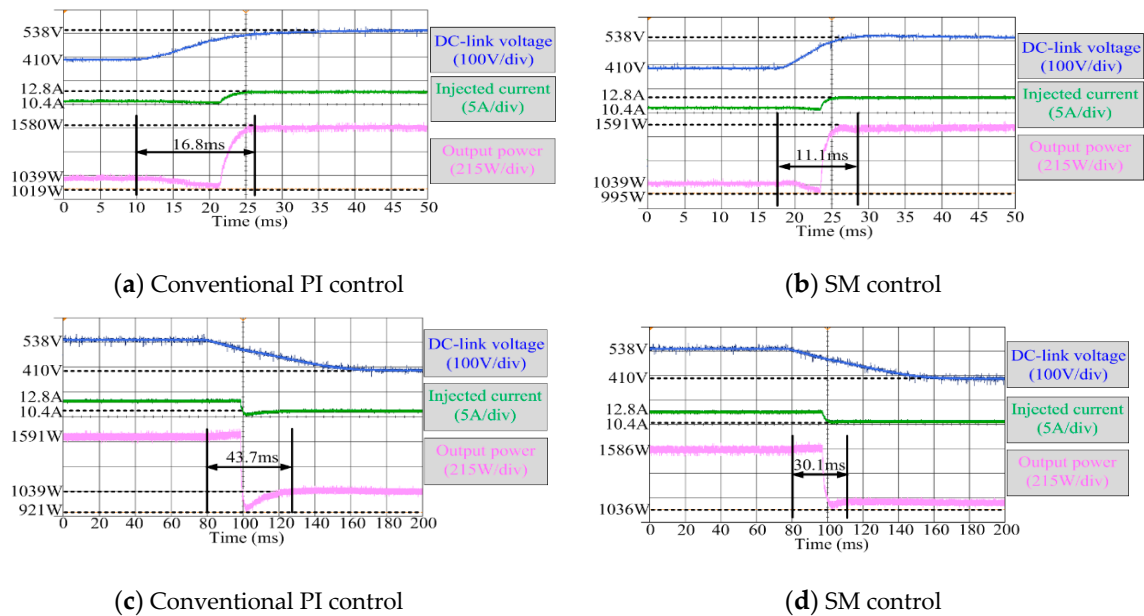
Figure 4. The experimental waveforms of the DC grid voltage, the injected current, and the output power of the entire WEC system for wind speeds altering from 6.6 to 7.9 m/s and vice versa.

The experiments were also carried out with a random wind profile within the wind speed between 6.6 m/s and 7.9 m/s. The results are depicted in Figure 5. A comparison of the energy harvested over 50 s of the WEC system controlled by the two control schemes exhibit the SM control for both MPPT controllers which can harvest approximately 0.44% more energy than the conventional PI control, as shown in Figure 6.

(**a**) Conventional PI control   (**b**) SM control
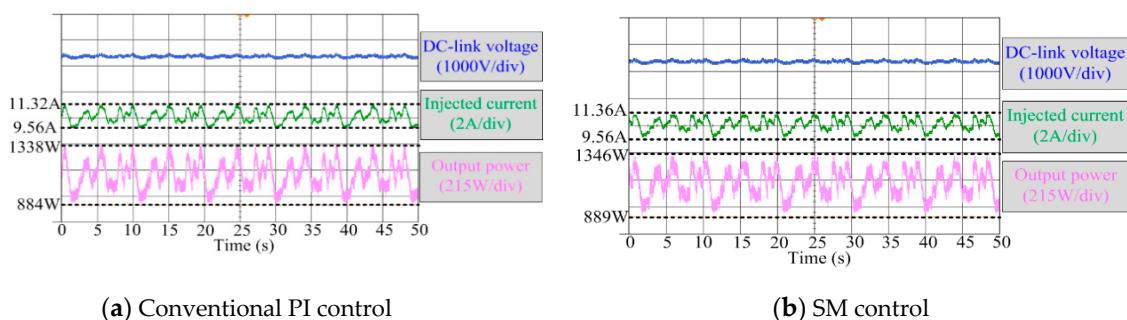
Figure 5. The experimental waveforms of the DC grid voltage, injected current, and output power of the entire WEC system for random wind profile under (**a**) proportional-integral (PI) and (**b**) sliding mode (SM) control.

Figure 6. Additional energy harvested of the WEC system with a random wind profile by the SM control than the conventional PI control.

In conclusion, the experimental results from this study validate that the energy harvesting property of renewable systems that have a fluctuating source, can be better improved using SM control compared to using conventional optimally-tuned PI control. SM control provides better dynamic tracking of the MPPT position for varying input and load conditions than linear control.

3. Case Study 2-SM Control of SS-Compensated WPT Systems with Renewable Energy Sources

In [38], SM control was designed for an SS-compensated WPT system to achieve maximum energy efficiency as well as output voltage regulation. The transmitter of the SS-compensated WPT consists of a full-bridge high-frequency DC/AC resonant inverter (S_1 to S_4) being controlled by a perturb-and-observation (P and O) phase-displacement control to minimize the input current from the renewable source, thereby achieving minimum input power. The receiver of the SS-compensated WPT consists of a buck-boost converter being controlled by a PI control or a SM control to dynamically match the optimal load condition. This section presents a brief discussion on the investigation.

The schematic diagram of a typical two-stage SS-compensated WPT system is plotted in Figure 7. The renewable source provides a time-varying DC power supply that may be fluctuating in amplitude with respect to solar irradiance, temperature, and load conditions. L_1 and L_2 represent the wireless power transmitter and receiver coil, respectively; C_1 and C_2 are the series compensation capacitors; and R_{p1} and R_{p2} are the equivalent parasitic resistance of the transmitter and receiver coil, respectively. The output of the receiver coil is connected to a full-bridge high-frequency rectifier diode circuit comprising D_1 to D_4 with storage capacitor C_b. Controller 1 is a P and O phase-displacement control for achieving minimum input power of the variable renewable source via the regulation of the zero-state phase angle of the output voltage of the DC/AC inverter V_{in} (schematics of Controller 1 can be found in [38]). Controller 2 is for regulating the output voltage the buck-boost converter and in this study, both the conventional PI control and the SM control are adopted for comparison.
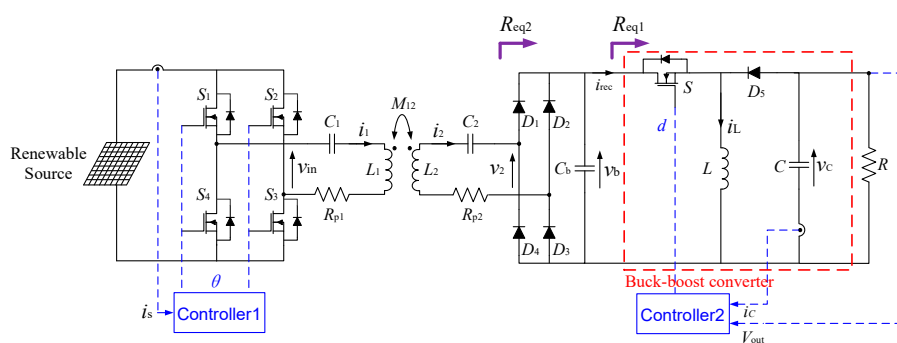
Figure 7. Schematic diagram of a typical two-stage SS-compensated wireless power transfer (WPT) system.

Conventionally, the PI control is adopted to regulate the buck-boost converter of the receiver,

$$\Delta u(k) = K_{\mathrm{p}} \Delta e(k) + K_{\mathrm{i}} e(k) \tag{16}$$

where $\Delta u(k) = u(k) - u(k-1)$ is the control signal increment; $e(k) = V_{\mathrm{ref}} - V_{\mathrm{out}}$ is the voltage error between the reference and the output voltage; and $\Delta e(k) = e(k) - e(k-1)$ is the voltage erroring increment. The control signal $u(k)$ is obtained by adding the control signal increment $\Delta u(k)$ to the control signal $u(k-1)$. The tuning coefficients K_{p} and K_{i} are tuned by the trial-and-error method.

However, the output voltage of the WPT system controlled by the conventional PI control (a typical linear control) can suffer from high overshoot/undershoot and long settling time during the dynamics, such as load-point change and P and O searching process of the phase-displacement control for the full-bridge inverter. To overcome such issues, SM control can be adopted for the buck-boost converter. The control variables $x(k)$ of the SM control can be expressed in the following form:

$$x(k) = \begin{bmatrix} x_1(k) \\ x_2(k) \\ x_3(k) \end{bmatrix} = \begin{bmatrix} V_{\mathrm{ref}} - V_{\mathrm{out}}(k) \\ \frac{1}{T_{\mathrm{s1}}} [V_{\mathrm{out}}(k) - V_{\mathrm{out}}(k+1)] \\ T_{\mathrm{s1}} \sum\limits_{j=0}^{k-1} [V'_{\mathrm{ref}} - V_{\mathrm{out}}(j)] \end{bmatrix} \tag{17}$$

The state-space model for the SM control can be further derived as:

$$x(k+1) = \begin{bmatrix} 1 & T_{\mathrm{s1}} & 0 \\ 0 & 1 - \frac{T_{\mathrm{s1}}}{RC} & 0 \\ T_{\mathrm{s1}} & 0 & 1 \end{bmatrix} \begin{bmatrix} x_1(k) \\ x_2(k) \\ x_3(k) \end{bmatrix} + \begin{bmatrix} 0 \\ \frac{T_{\mathrm{s1}} V_{\mathrm{out}}(k)}{LC} - \frac{T_{\mathrm{s1}} V_{\mathrm{out}}(k)}{LC} u(k) \\ 0 \end{bmatrix} \tag{18}$$

The sliding surface of the SM control is given as:

$$S(k) = \alpha_1 x_1(k) + \alpha_2 x_2(k) + \alpha_3 x_3(k) \tag{19}$$

where α_1, α_2, and α_3 are the sliding coefficients (i.e., $\alpha_1 > 0$, $\alpha_2 > 0$ and $\alpha_3 > 0$). Then, the equivalent control signal $u_{\mathrm{eq}}(k)$ can be obtained by letting $S(k+1) = S(k)$,

$$u_{\mathrm{eq}}(k) = 1 - \frac{K_1}{V_{\mathrm{ref}}} + \frac{K_1}{V_{\mathrm{out}}(k)} + \frac{K_2 i_c(k)}{V_{\mathrm{out}}(k)} \tag{20}$$

where $K_1 = \frac{\alpha_3 LC V'_{\mathrm{ref}}}{\alpha_2}$ and $K_2 = \frac{L}{RC} - \frac{\alpha_1 L}{\alpha_2}$ are the tuning coefficients of the SM control. The equivalent control signal satisfies $0 \leq u_{\mathrm{eq}}(k) < 1$, which equalizes the duty ratio $d(k)$ of the pulse-width modulation. The sliding coefficients α_1, α_2, and α_3 are optimally tuned based on the guidelines in [1].

The results of the dynamic performance of the system between the conventional PI control and the SM control for the SS-compensated WPT system are shown in Figures 8 and 9. The PI control is designed under the operating condition when V_{in} has no zero-state in its output voltage waveform, i.e., zero-state phase angle is 0. From Figure 8a, it is shown that in the event that the zero-state phase angle of V_{in} is step-changed from 120° to 100°, the overshoot of the output voltage V_{out} of the buck-boost converter controlled by the conventional PI control is approximately 2.5 V and the settling time is approximately 151.8 ms during the transient state. For the same conditions, the overshoot of V_{out} of the buck-boost converter controlled by the SM control is approximately 2 V and the settling time is approximately 48 ms, as shown in Figure 8b. The overshoot is reduced by approximately 20% and the settling time is reduced by approximately 68.4%.
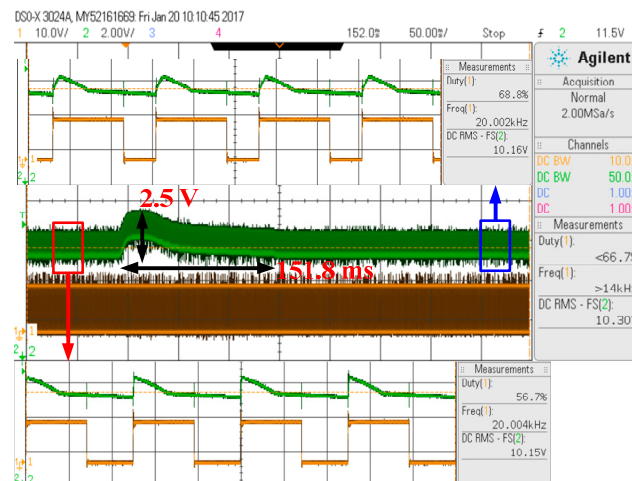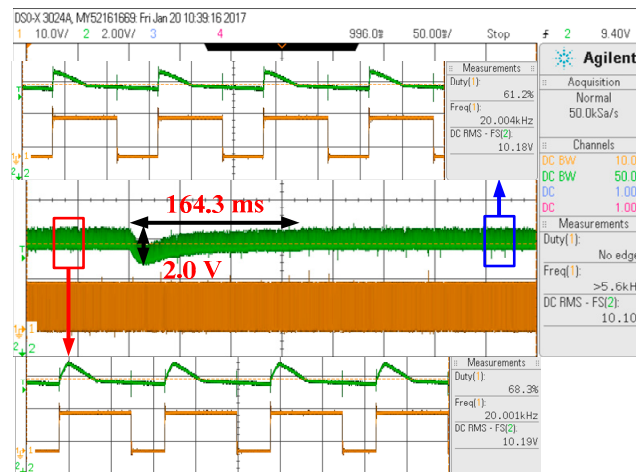
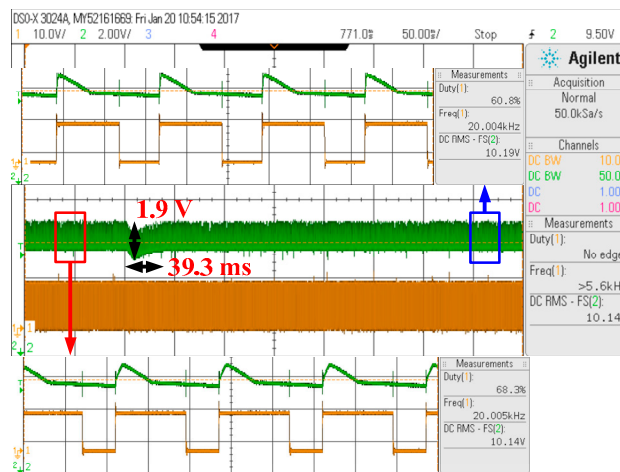(**a**) Conventional PI control
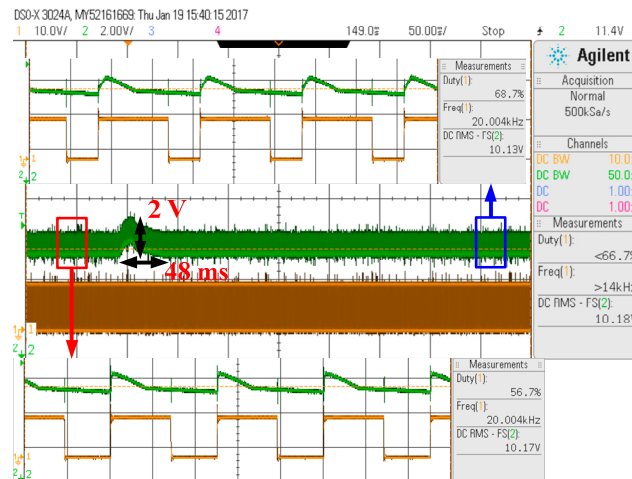
(**b**) SM control

Figure 8. The waveforms of V_{out} and the switching signals when the phase displacement is altered from 120° to 100°.

For the case of step-changing, the zero-state phase angle of V_{in} from 100° to 110°, an undershoot of V_{out} of approximately 2 V is present and the settling time is approximately 164.3 ms with the PI control (see Figure 9a), while it is approximately 1.9 V and approximately 39.3 ms with the SM control. The same experiment is applied for other step change conditions and the results indicate that with the SM control, the output voltage can always have a lower overshoot/undershoot and settling time as compared to PI control.

In conclusion, this study shows and validates that SM control performs better dynamic regulation of the output voltage than PI control in systems, in terms of lowering overshoots and having faster settling time in the event of the variation of the renewable source. This is particularly important in modern clean energy environments such as that using WPT for electric vehicle charging. The improvement can prevent the load suffering from undesirable overshoot/undershoot during dynamics and gives better over-voltage and under-voltage protection to the loads and complementing circuitries.

(**a**) Conventional PI control

(**b**) SM control

Figure 9. The waveforms of V_{out} and the switching signals when the phase displacement is altered from 100° to 110°.

4. Case Study 3-SM Control of Multiple Energy Storage Systems in DC Microgrids

In [40], a two-layer hierarchical control scheme was adopted in a system with multiple ESS to mitigate the distribution power loss on the transmission power cables of standalone DC microgrids. The hierarchical control comprises a centralized model predictive control (CMPC) with adaptive weighting factors and multiple local PI controls. The CMPC is a secondary control that generates bus voltage references for the local PI control of each ESS based on the optimization of the flow power in the standalone DC microgrid. The multiple local PI controllers are primary controllers that track the references provided by the CMPC to achieve the overall functions. The two-layer hierarchical control scheme coordinates the various ESS to reduce the power loss on the transmission power cables of the standalone DC microgrid, while simultaneously regulating the DC bus voltages within the tolerances (i.e., ±5% tolerance). However, the hierarchical control scheme reported in [40] only guaranteed the bus voltages to be regulated within a ±5% tolerance in a steady state, while the overshoot and undershoot during transient states may exceed the tolerance. This may cause unwanted electrical tripping of the microgrids, especially when voltage level of the renewable energy sources (RES) fluctuate widely and randomly on certain occasions. In this section, the simulation results and discussions based on the use of SM control in replacement of the conventional PI control adopted in the hierarchical control scheme reported in [40], are presented. The SM control is adopted as a local control for

the grid-connected converters of the ESS. The structure of the investigated 380 V five-bus standalone DC microgrid is depicted in Figure 10. The RES 1 and RES 2 are integrated at Bus 1 and Bus 5, respectively. Three ESS are installed at Buses 1, 3, and 4, respectively. The grid-connected converters of the ESS are non-isolated boost converters shown in Figure 11. The overall control block diagram of multiple ESS in the five-bus standalone DC microgrid is shown in Figure 12. For fair comparison, both the conventional PI control and the SM control are adopted as local controls to regulate the bus voltage and to track the bus voltage reference generated by the CMPC (schematics of the CMPC can be found in [40]).

For the conventional PI control, the control signal is

$$u_{\text{PI}} = K_{\text{pI}}(i_{\text{Lref}} - i_{\text{L}}) + K_{\text{iI}} \int_o^t (i_{\text{Lref}} - i_{\text{L}})dt \tag{21}$$

where the inductor current reference is generated based on

$$i_{\text{Lref}} = K_{\text{pV}}(V_{\text{busref}} - V_{\text{bus}}) + K_{\text{iV}} \int_o^t (V_{\text{busref}} - V_{\text{bus}})dt \tag{22}$$

The tuning coefficients of the conventional PI control (i.e., K_{pI}, K_{iI}, K_{pV}, and K_{iV}) are optimized offline by the genetic algorithm (GA). The schematic diagram of the parameter tuning of the conventional PI control is depicted in Figure 13. Here, V_{err} is the difference between the bus voltage reference and the bus voltage (i.e., $V_{\text{err}} = V_{\text{busref}} - V_{\text{bus}}$).

For the SM control, the control variables are:

$$x(k) = \begin{bmatrix} x_1 \\ x_2 \\ x_3 \end{bmatrix} = \begin{bmatrix} i_{\text{Lref}} - i_{\text{L}} \\ V_{\text{busref}} - V_{\text{bus}} \\ \int(i_{\text{Lref}} - i_{\text{L}})dt + \int(V_{\text{busref}} - V_{\text{bus}})dt \end{bmatrix} \tag{23}$$

The sliding surface of the SM control is given as:

$$s = \alpha_1 x_1 + \alpha_2 x_2 + \alpha_3 x_3 \tag{24}$$

where α_1, α_2, and α_3 are the sliding coefficients (i.e., $\alpha_1 > 0$, $\alpha_2 > 0$ and $\alpha_3 > 0$). Then, the equivalent control signal u_{SM} can be obtained by letting $S \cdot \dot{S} < 0$ to give:

$$u_{\text{SM}} = 1 - \frac{K_2 \frac{V_{\text{bus}}}{R_{\text{L}}} - V_{\text{bat}} + K_3(V_{\text{busref}} - V_{\text{bus}}) - K_3(i_{\text{Lref}} - i_{\text{L}})}{K_2 i_{\text{L}} - V_{\text{bus}}} \tag{25}$$

where $K_1 = \frac{\alpha_3 L(K+1)}{\alpha_1}$, $K_2 = \frac{L}{C}\left(K + \frac{\alpha_2}{\alpha_1}\right)$, and $K_3 = \frac{\alpha_3 L}{\alpha_1}$. The sliding coefficients α_1, α_2, α_3, and K are optimally tuned based on the guidelines in [1].
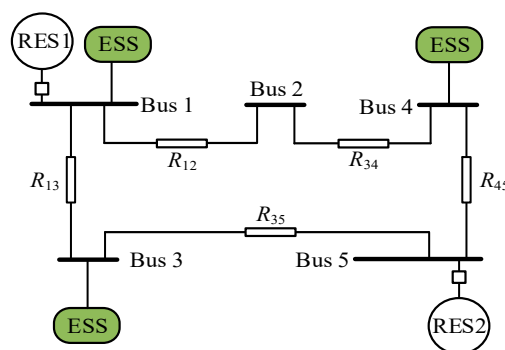

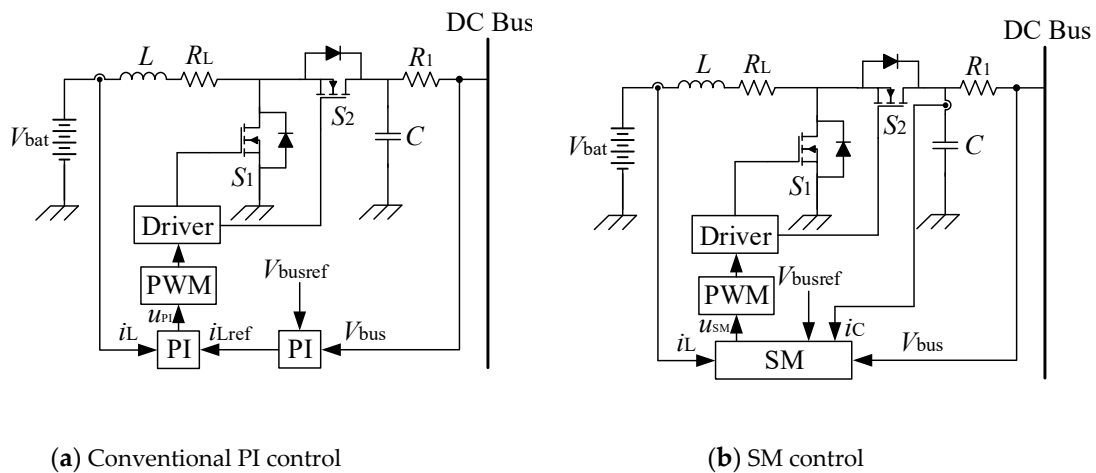**Figure 10.** The structure of the investigated five-bus standalone DC microgrid.

(**a**) Conventional PI control

(**b**) SM control

Figure 11. The circuitry and control of the grid-connected converters for energy storage systems (ESS).
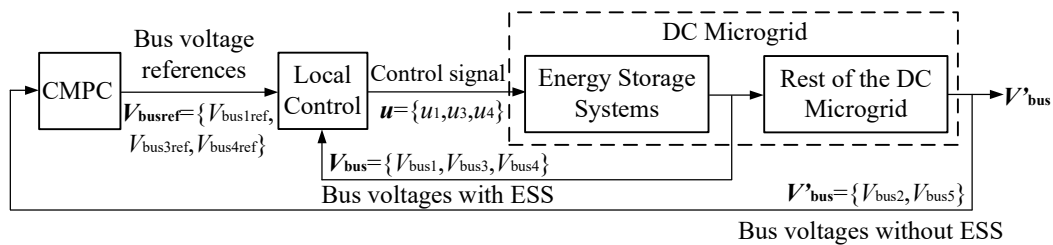

Figure 12. Overall control block diagram of multiple ESS in the five-bus standalone DC microgrid.
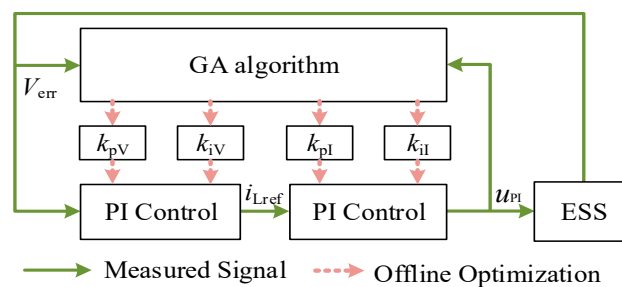

Figure 13. Schematic diagram of the parameter tuning of the conventional PI control.

Figure 14 shows the comparison of the energy loss reduction of the five-bus standalone DC microgrid over 5 s (1–6 s) based on the conventional PI control and the SM control. The difference between the two control schemes are negligible, which means that both the conventional PI control and the SM control are tracking the references generated by CMPC rapidly and have similar effects in reducing the distribution power loss. The waveforms of the bus voltages over a time period of 5 s under both control schemes are shown in Figure 15. Apparently, the voltages of Bus 1 during the intervals of 1–2 s, 4–5 s, and 5–6 s, Bus 2 during the intervals of 2–3 s and 5–6 s, Bus 3 during the interval of 4–5 s, Bus 4 during the intervals of 2–3 s and 5–6 s, and Bus 5 during the interval of 4–5 s are all out of the ±5% tolerance during transient when the grid-connected converters of ESS are using the conventional PI control. However, all the bus voltages are within the tolerance during transient when they are controlled using the SM control. This is important if grid protection is of concern and when achieving stringent voltage regulation is valued. It is apparent that SM control exhibits strength in achieving both features in this case.
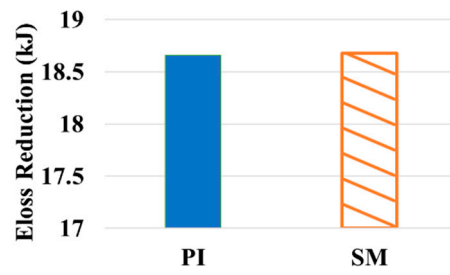
Figure 14. The energy loss reduction of the DC microgrid with PI and SM control.
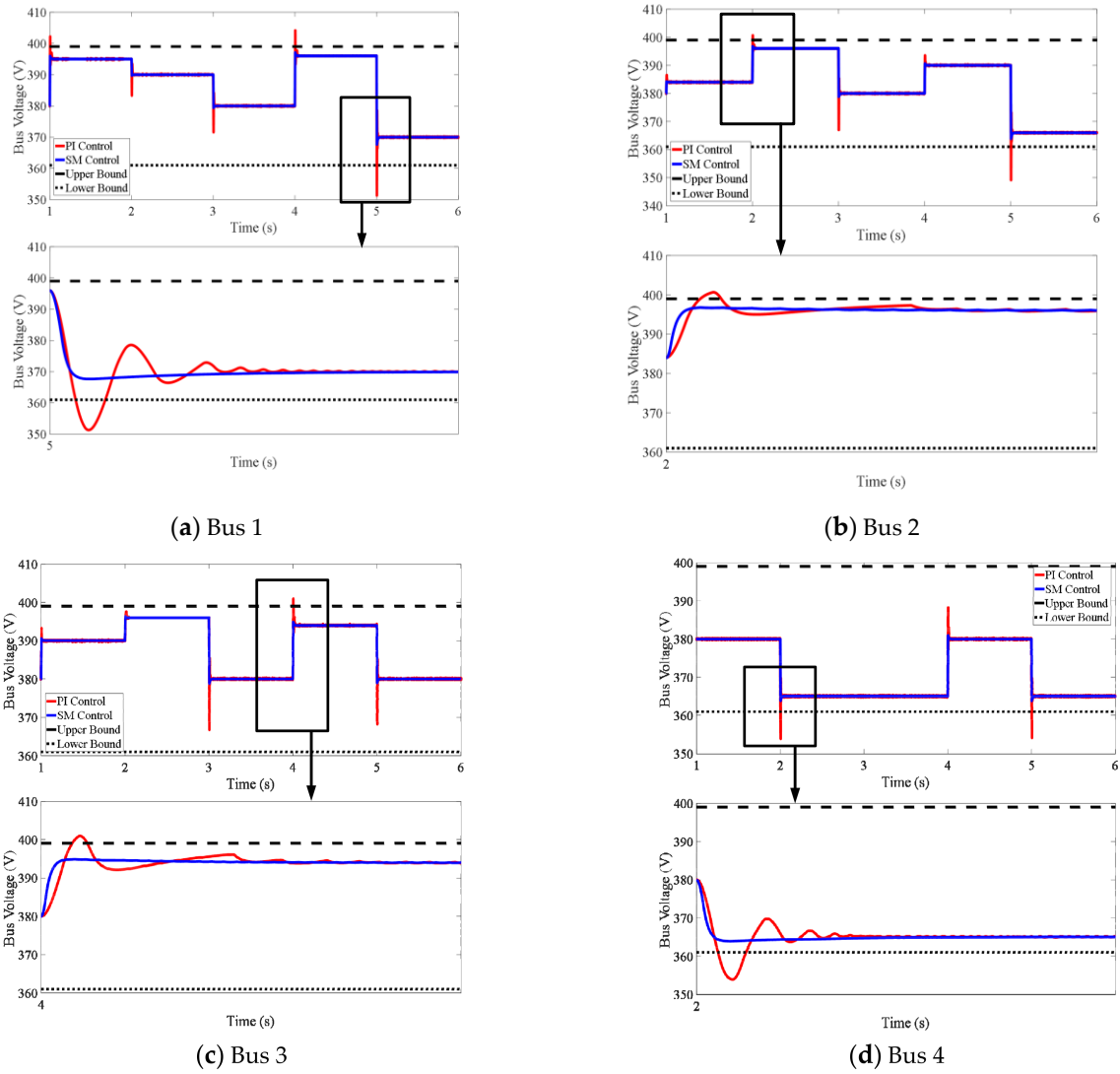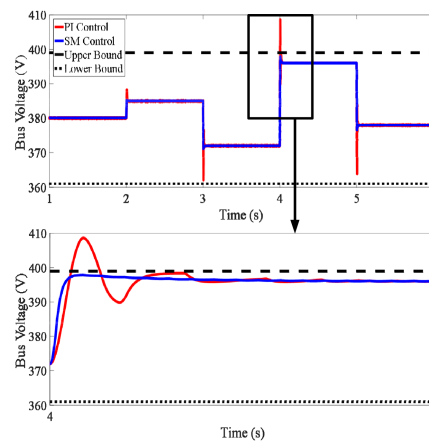

(**a**) Bus 1

(**b**) Bus 2

(**c**) Bus 3

(**d**) Bus 4

Figure 15. *Cont*.

(**e**) Bus 5

Figure 15. Bus voltages of the DC microgrid over a simulation period of 5 s with both PI and SM control.

5. Conclusions and Future Discussions

Sliding mode control is a well-established control method that has been widely applied in power converters for its properties of high robustness against parameter uncertainties, fast dynamic responses, high flexibility in the design, and easy implementations as compared to other nonlinear control techniques. This paper further presented the recent developments and trends of sliding mode control applications to power-electronics based renewable energy systems. Notably, in addition to achieving high power quality, such as high voltage and frequency stability, high power factor, and low voltage and current harmonics, the applications of sliding mode control can be extended to include efficiency improvement and better load protections of renewable energy systems, via the exploitation of the fast-dynamic-response property of sliding mode control. The case studies provided in the paper have shown that sliding mode control can increase the energy harvested from renewable sources and achieves better dynamic regulation of output and bus voltages. This, thereby, protects the load and the system from possible large overshoot/undershoot that may arise as a result of poor control of the system or that of any constituting component.

Most of the present applications of sliding mode control for power converters in renewable energy systems focus on the single-input-single-output pulse-width-modulation-based converters. The sliding mode control may be further applied for multiple-input-multiple-output pulse-width-modulation-based converters, which include single multiple-input-multiple-output converters, e.g., multi-port converters for high voltage step-up/down applications, and multiple single-input-single-output converters distributed and installed in a network. The single multiple-input-multiple-output converters are widely used in data centers and other isolated grids, e.g., grids in electric ships. The multiple single-input-single-output converters are widely adopted for distributed renewable energy sources and energy storage systems in microgrids. The sliding mode control designs for multiple-input-multiple-output pulse-width -modulation-based converters may consider hierarchical structures, which comprises two or more layers of sliding mode control.

Author Contributions: Conceptualization, Y.Y. and S.C.T.; methodology, Y.Y. and S.C.T.; software, Y.Y.; validation, Y.Y. and S.C.T.; formal analysis, Y.Y. and S.C.T.; investigation, Y.Y. and S.C.T.; resources, S.C.T.; data curation, Y.Y.; writing—original draft preparation, Y.Y.; writing—review and editing, S.C.T.; supervision, S.C.T.; project administration, S.C.T.

References

1. Tan, S.C.; Lai, Y.M.; Tse, C.K. *Sliding Mode Control of Switching Power Converters-Techniques and Implementation*; CRC Press: Boca Raton, FL, USA, 2012.
2. Emelyanov, S.V. *Variable Structure Control Systems*; Nauka: Moscow, Russia, 1967. (In Russian)
3. Itkis, Y. *Control Systems of Variable Structure*; Wiley: New York, NY, USA, 1976.
4. Utkin, V.I. *Sliding Mode and Their Application in Variable Structure Systems*; Mir Publisher: Moscow, Russia, 1978.
5. Utkin, V.I. Variable structure systems with sliding modes. *IEEE Trans. Autom. Control* **1977**, *22*, 212–222. [CrossRef]
6. Sarpturk, S.Z.; Istefanopulos, Y.; Kaynak, O. On the stability of discrete-time sliding mode control system. *IEEE Trans. Autom. Control* **1987**, *32*, 930–932. [CrossRef]
7. Sira-Ramirez, H.; Llanes, S.O. Adaptive dynamical sliding mode control via backstepping. In Proceedings of the 32nd IEEE Conference on Decision and Control, San Antonio, TX, USA, 15–17 December 1993; pp. 1422–1427.
8. Wheeler, G.; Su, C.H.; Stepanenko, Y. A sliding mode controller with improved adaption laws for the upper bounds on the norm of uncertainties. *Automatica* **1998**, *34*, 1657–1661. [CrossRef]
9. Feng, Y.; Yu, X.H.; Man, Z.H. Non-singular terminal sliding mode control of rigid manipulator. *Automatica* **2002**, *38*, 281–288. [CrossRef]
10. Choi, H.S.; Park, Y.H.; Cho, Y.S.; Lee, M.H. Global sliding mode control. *IEEE Control Syst. Mag.* **2001**, *21*, 27–35.
11. Lu, Y.S.; Chen, J.S. A self-organizing fuzzy sliding-mode controller design for a class of nonlinear servo systems. *IEEE Trans. Ind. Electron.* **1994**, *41*, 492–502.
12. Yoo, B.; Ham, W. Adaptive fuzzy sliding mode control of nonlinear system. *IEEE Trans. Fuzzy Syst.* **1998**, *6*, 315–321.
13. Bilalović, F.; Mušić, O.; Šabanović, A. Buck converter regulator operating in the sliding mode. In Proceedings of the Seventh International Conference on Power Conversion, Dallas, TX, USA, 7–8 February 2007; pp. 331–340.
14. Venkataramanan, R.; Šabanović, A.; Ćuk, S. Sliding mode control of DC-to-DC converters. In Proceedings of the IEEE Conference on Industrial Electronics, Control and Instrumentations, Dubrovnik, Croatia, 15–18 September 2002; pp. 251–258.
15. Huang, S.P.; Xu, H.Q.; Liu, Y.F. Sliding-mode controlled of DC/DC converters. In Proceedings of the IEEE Power Electronics Specialists Conference Record, Milwaukee, WI, USA, 26–29 June 1989; pp. 124–129.
16. Fossas, E.; Martínez, L.; Ordinas, J. Sliding mode control reduces audiosusceptibility and load perturbation in the Ćuk converter. *IEEE Trans. Circuits Syst. Part I* **1992**, *39*, 847–849. [CrossRef]
17. Malesani, L.; Rossetto, L.; Spiazzi, G.; Tenti, P. Performance optimization of Ćuk converters by sliding-mode control. *IEEE Trans. Power Electron.* **1995**, *10*, 302–309. [CrossRef]
18. Martínez-Salamero, L.; Calvente, J.; Giral, R.; Poveda, A.; Fossas, E. Analysis of a bidirectional coupled-inductor Ćuk converter operating in sliding mode. *IEEE Trans. Circuits Syst. Part I* **1998**, *45*, 355–363. [CrossRef]
19. Mattavelli, P.; Rossetto, L.; Spiazzi, G. Small-signal analysis of DC-DC converters with sliding mode control. *IEEE Trans. Power Electron.* **1997**, *12*, 96–102. [CrossRef]
20. Castilla, M.; De Vicuna, L.C.; Lopez, O.; Matas, J. On the design of sliding mode control schemes for quantum resonant converters. *IEEE Trans. Power Electron.* **2000**, *15*, 960–973. [CrossRef]
21. Donoso-Garcia, P.F.; Cortizo, P.C.; De Menezes, B.R.; Severo Mendes, M.A. Sliding mode control for current distribution on DC-to-DC converters connected in parallel. In Proceedings of the IEEE Power Electronics Specialists Conference Record, Baveno, Italy, 23–27 June 1996; pp. 1513–1518.
22. Giral, R.; Martínez-Salamero, L.; Leyva, R.; Maixe, J. Sliding-mode control of interleaved boost converters. *IEEE Trans. Circuits Syst. Part I* **1998**, *47*, 1330–1339.
23. López, M.; De-Vicuňa, L.G.; Castilla, M.; Gaya, P.; López, O. Current distribution control design for paralleled DC/DC converters using sliding-mode control. *IEEE Trans. Ind. Electron.* **2004**, *45*, 1091–1100. [CrossRef]
24. Sira-Ramirez, H.; Rios-Bolivar, M. Sliding mode control of DC-to-DC power converters via extended linearization. *IEEE Trans. Circuits Syst. Part I* **1994**, *41*, 652–661. [CrossRef]
25. Escobar, G.; Ortega, R.; Sira-Ramirez, H.; Vilain, J.P.; Zein, I. An experimental comparison of several nonlinear controllers for power converters. *IEEE Control Syst. Mag.* **1999**, *19*, 66–82.

26. Bashash, S.; Fathy, H.K. Modeling and control of aggregate air conditioning loads for robust renewable power management. *IEEE Trans. Control Syst. Technol.* **2013**, *21*, 1318–1327. [CrossRef]

27. Moré, J.J.; Puleston, P.F.; Kunusch, C.; Fantova, M.A. Development and implementation of a supervisor strategy and sliding mode control setup for fuel-cell-based hybrid generation systems. *IEEE Trans. Energy Convers.* **2015**, *30*, 218–225. [CrossRef]

28. Baghaee, H.R.; Mirsalim, M.; Gharegpetian, G.B.; Talebi, H.A. A decentralized power management and sliding mode control strategy for hybrid AC/DC microgrids including renewable energy resources. *IEEE Trans. Ind. Informat.* **2017**, in press. [CrossRef]

29. Wang, C.; Mi, Y.; Fu, Y.; Wang, P. Frequency control of an isolated micro-grid using double sliding mode controllers and disturbance observer. *IEEE Trans. Smart Grid* **2018**, *9*, 923–930. [CrossRef]

30. Liu, J.; Jiang, S.; Cao, D.; Lu, X.; Peng, F.Z. Sliding mode control of quasi-z-source inverter with battery for renewable energy system. In Proceedings of the IEEE Energy Conversion Congress and Exposition, Phoenix, AZ, USA, 16–21 September 2011; pp. 3665–3671.

31. Tabart, Q.; Vechiu, I.; Etxeberria, A.; Bacha, S. Hybrid energy storage system microgrids integration for power quality improvement using four-leg three-level NPC inverter and second-order sliding mode control. *IEEE Trans. Ind. Electron.* **2018**, *65*, 424–435. [CrossRef]

32. Beltran, B.; Tarek, A.A.; Benbouzid, M.E.H. High-order sliding-mode control of variable-speed wind turbines. *IEEE Trans. Ind. Electron.* **2009**, *56*, 3314–3321. [CrossRef]

33. Hoseini, S.K.; Pouresmaeil, E.; Hosseinnia, S.H.; Catalão, J.P.S. A control approach for the operation of DG units under variations of interfacing impedance in grid-connected mode. *Int. J. Electr. Power Energy Syst.* **2016**, *74*, 1–8. [CrossRef]

34. Hoseini, S.K.; Pouresmaeil, E.; Adabi, J.; Catalão, J.P.S. Stable integration of power electronics-based DG links to the utility grid with interfacing impedance uncertainties. In Proceedings of the Doctoral Conference on Computing, Electrical and Industrial Systems, Costa de Caparica, Portugal, 28 March 2015; pp. 502–511.

35. Haroun, R.; Aroudi, A.E.; Cid-Pastor, A.; Garcia, G.; Olalla, C.; Martínez-Salamero, L. Impedance matching in photovoltaic systems using cascaded boost converters and sliding-mode control. *IEEE Trans. Power Electron.* **2015**, *30*, 3185–3199. [CrossRef]

36. Yang, Z.; Ho, C.N.M.; Siu, K.K.M. A fast and accurate MPP control technique using boundary controller for PV applications. In Proceedings of the IEEE Applied Power Electronics Conference and Exposition, Anaheim, FL, USA, 26–30 March 2017; pp. 2822–2829.

37. Yang, Y.; Mok, K.T.; Tan, S.C.; Hui, S.Y.R. Nonlinear dynamic power tracking of low-power wind energy conversion system. *IEEE Trans. Power Electron.* **2015**, *30*, 5223–5236. [CrossRef]

38. Yang, Y.; Zhong, W.X.; Kiratipongvoot, S.; Tan, S.C.; Hui, S.Y.R. Dynamic improvement of series-series compensated wireless power transfer systems using discrete sliding mode control. *IEEE Trans. Power Electron.* **2018**, *33*, 6351–6360. [CrossRef]

39. Li, K.; Yang, Y.; Tan, S.C.; Hui, S.Y.R. Sliding-mode-based direct power control of dual-active-bridge DC-DC converters. In Proceedings of the IEEE Applied Power Electronics Conference and Exposition, Anaheim, CA, USA, 17–21 March 2019; pp. 188–192.

40. Yang, Y.; Tan, S.C.; Hui, S.Y.R. Mitigating distribution power loss of DC microgrids with DC electric spring. *IEEE Trans. Smart Grid* **2018**, *9*, 5897–5906. [CrossRef]